

Dimensional evolution between one- and two-dimensional topological phases

Huaiming Guo*, Yang Lin

Department of Physics, Beihang University, Beijing, 100191, China

Shun-Qing Shen

Department of Physics, The University of Hong Kong, Pokfulam Road, Hong Kong

Dimensional evolution between one- ($1D$) and two-dimensional ($2D$) topological phases is investigated systematically. The crossover from a $2D$ topological insulator to its $1D$ limit shows oscillating behavior between a $1D$ ordinary insulator and a $1D$ topological insulator. By constructing a $2D$ topological system from a $1D$ topological insulator, it is shown that there exist possibly weak topological phases in $2D$ time-reversal invariant band insulators, one of which can be realized in anisotropic systems. The topological invariant of the phase is $Z_2 = 0$. However the edge states may appear along specific boundaries. It can be interpreted as arranged $1D$ topological phases, and have symmetry-protecting nature as the corresponding $1D$ topological phase. Robust edge states can exist under specific conditions. These results provide further understanding on $2D$ time-reversal invariant insulators, and can be realized experimentally.

I. INTRODUCTION

Topological insulator (TI) is a novel quantum state of matter, which is determined by the topological properties of its band structure. It has generated great interests in the field of condensed matter physics and material science due to its many exotic electromagnetic properties and possible potential applications²⁻⁵. Its discovery also deepens understanding on the time-reversal invariant band insulators. In two dimensions, ordinary insulator and quantum spin Hall insulator are characterized by a Z_2 invariant ν : $\nu = 0$ for a conventional insulator and $\nu = 1$ for a quantum spin Hall insulator^{6,7}. In three dimensions ($3D$) time-reversal invariant band insulators can be classified into 16 topological classes distinguished by four Z_2 topological invariants, and thus the ordinary insulator is distinguished from 'weak' and 'strong' TIs^{8,9}.

The $3D$ TIs have been proposed and verified in many materials¹⁰⁻¹⁴. However the $2D$ TIs have only been realized in HgTe/CdTe and InAs/GaSb/AlSb quantum well systems¹⁵⁻¹⁷. Theoretical studies have suggested that the $2D$ TI may be achieved in a thin film of $3D$ TI. In the thin film, the quantum tunneling between the two surfaces generates a hybridized gap at the Dirac point. Depending on the thickness of the quantum wells, the system oscillates between an ordinary insulator and quantum spin Hall insulator^{18,19}. Typical TI materials, such as Bi_2Te_3 and Bi_2Se_3 have a layered structure consisting of weakly coupled quintuple layers, which makes it relatively easy to grow high quality crystalline thin films using molecular beam epitaxy. Until now the thin films of $3D$ TIs have been successfully fabricated experimentally and the gap-opening has been observed^{20,21}. This paves the way to realize the quantum spin Hall insulator from the present various $3D$ TIs, which will greatly enlarge the family of $2D$ TIs. Furthermore by introducing ferromagnetism in thin film, the quantum anomalous Hall effect can be realized, which has been experimentally confirmed in magnetic TIs of Cr-doped $(Bi, Sb)_2Te_3$ ^{22,23}.

Also it has been shown that the Chern number of quantum anomalous Hall effect can be higher than one by tuning exchange field or sample thickness^{24,25}. Compared to the $3D$ strong TIs, the weak TIs are related to the topological property of the lower dimensions in a more direct way, since it can be interpreted as layered $2D$ quantum spin Hall insulator. Though no weak TIs have been reported experimentally, they are expected to have interesting physical properties²⁶⁻³⁰. Besides the studies on the $2D$ limit of $3D$ TIs, recently a theoretical formalism has been developed to show that a $3D$ TI can be designed artificially via stacking $2D$ layers³¹. It provides controllable approach to engineer 'homemade' TIs and overcomes the limitation imposed by bulk crystal geometry.

The above studies show the connection between the $2D$ and $3D$ TIs. It is notable that recently there are increasing interests in $1D$ topological phases³²⁻³⁵. Specially they have been studied experimentally using ultra-cold fermions trapped in the optical superlattice and photons in photonic quasicrystals^{36,37} and metamaterials³⁸. With the developments of these techniques, various $1D$ models with topological properties may be realized³⁹. Also these techniques can be easily extended to $2D$ or $3D$ cases. It is also desirable to study the $1D$ topological phase in real materials. A natural thought is to narrow a $2D$ TI and the narrow strip may be a $1D$ TI. Also a formalism on how to construct $2D$ TIs from $1D$ ones is needed. The underlying question is the connections between the $1D$ and $2D$ TIs.

In the paper, the question is studied systematically. It is found that the crossover from the $2D$ quantum spin Hall insulator to its $1D$ limit shows oscillatory behavior between a $1D$ ordinary insulator and $1D$ TI. Generally the $2D$ TI is a 'genuine' $2D$ phase and cannot be understood simply from the corresponding $1D$ phases. However by arranging $1D$ TIs, it is found that there exists a $2D$ weak topological phase in anisotropic systems. In contrast to the quantum spin Hall insulator: the $2D$ weak TI has topological invariant $Z_2 = 0$; the edge states

are mid-gap ones and only appear along specific boundaries. These results provide further understanding on 2D time-reversal invariant insulators, and can be realized experimentally. The paper is organized as the following: In Sec.II, the model Hamiltonian is introduced to describe the 1D and 2D TIs; In Sec.III, an oscillatory crossover from 2D to 1D topological phases is observed; In Sec. IV, a 2D weak TI is identified by arranging 1D topological models; In Sec. V, the physical properties of the 2D weak TI are studied; Finally Sec. VI is the conclusion of the present paper.

II. THE 1D AND 2D TI MODELS

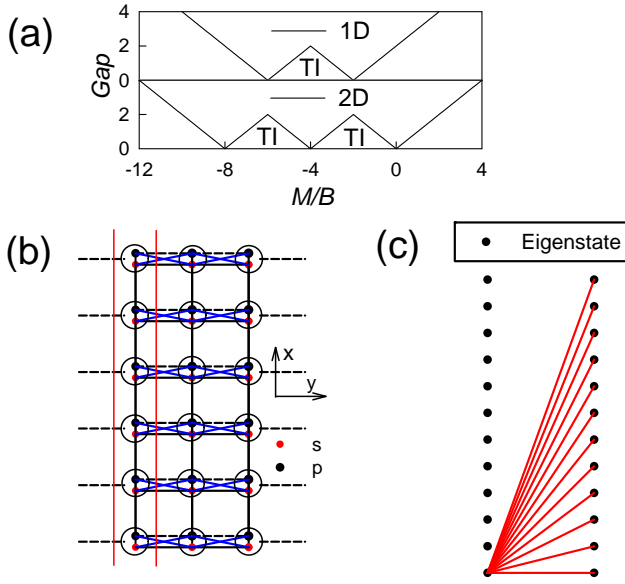


FIG. 1: (a) The phase diagram of the Hamiltonian Eq.(1) and Eq.(2). (b) The schematic diagram of the 2D model Eq.(1), in which the A -kind (blue solid lines) and B -kind (dashed and solid black lines) hoppings along y -direction are shown. (c) The real hopping between the NN chains are converted to the hopping between the eigenstates of the NN chains.

The starting point of the present work is the 2D tight-binding model for a quantum spin Hall insulator^{15,40},

$$\begin{aligned}
 H_{2D} = & \sum_i (M + 4B) \Psi_i^\dagger I \otimes \sigma_z \Psi_i \\
 & - \sum_{i,\hat{x}} B \Psi_i^\dagger I \otimes \sigma_z \Psi_{i+\hat{x}} - \sum_{i,\hat{y}} B \Psi_i^\dagger I \otimes \sigma_z \Psi_{i+\hat{y}} \\
 & - \sum_{i,\hat{x}} \text{sgn}(\hat{x}) i A \Psi_i^\dagger s_z \otimes \sigma_x \Psi_{i+\hat{x}} \\
 & - \sum_{i,\hat{y}} \text{sgn}(\hat{y}) i A \Psi_i^\dagger I \otimes \sigma_y \Psi_{i+\hat{y}}
 \end{aligned} \quad (1)$$

where I is the identity matrix and σ_j , s_j ($j = x, y, z$) are the Pauli matrices representing the orbit and spin,

respectively; $\Psi_i = (s_{i\uparrow}, p_{i\uparrow}, s_{i\downarrow}, p_{i\downarrow})^T$ with $s_{i\uparrow(\downarrow)}(p_{i\uparrow(\downarrow)})$ electron annihilating operator at site \mathbf{r}_i . The first term is the on-site potential, which has different signs for the s - orbit and p - orbit. The second and third terms are the hopping amplitudes among the s - orbits or p - orbits, which are differed by a sign. The third and fourth terms are the hopping amplitudes between the s - orbit and p - orbit electrons, which is due to the spin-orbit coupling. A and B are the hopping amplitudes and in the following of the paper we take B positive and set $A = 1$ as a unit of the energy scale. The Hamiltonian is invariant under time-reversal $\mathcal{T} = i s_y \otimes IK$. It belongs to the AII class and its topological property is described by a Z_2 index⁴¹. For $M > 0, M < -8B$ it is a trivial insulator. For $-8B < M < 0$ it is a quantum spin Hall insulator with the topological invariant $Z_2 = 1$. In the Hamiltonian, the subsystems of spin-up and -down are decoupled.

Based on the spin-up subsystem and reducing one dimension (such as the y - dimension), a 1D spinless topological model is obtained³³⁻³⁵,

$$\begin{aligned}
 H_{1D} = & \sum_i (M + 4B) \Psi_{i\uparrow}^\dagger \sigma_z \Psi_{i\uparrow} - \sum_{i,\hat{x}} B \Psi_{i\uparrow}^\dagger \sigma_z \Psi_{i+\hat{x}} \\
 & - \sum_{i,\hat{x}} \text{sgn}(\hat{x}) i A \Psi_{i\uparrow}^\dagger \sigma_x \Psi_{i+\hat{x}}.
 \end{aligned}$$

At half-filling, the system is a non-trivial insulator for $-6B < M < -2B$ and a trivial insulator for $M > -2B$ or $M < -6B$. In the momentum space it becomes: $H_{1D}(k) = [M + 4B - 2B \cos(k)] \sigma_z + 2A \sin(k) \sigma_x$. The Hamiltonian possesses a particle-hole symmetry $\sigma_x H_{1D}^*(k) \sigma_x = -H_{1D}(-k)$, a pseudo-time-reversal symmetry $\sigma_z H_{1D}^*(k) \sigma_z = H_{1D}(-k)$ and a chiral symmetry $\sigma_y H_{1D}(k) \sigma_y = -H_{1D}(k)$. It belongs to the BDI class and its topological invariant is a winding number ν , which is an integer⁴²⁻⁴⁴. The winding number of the Hamiltonian Eq.(2) is $\nu = 1$. In the case, it is equivalent to the Berry phase, which describes the electric polarization. The Berry phase in the k space is defined as: $\gamma = \oint \mathcal{A}(k) dk$ with the Berry connection $\mathcal{A}(k) = i \langle u_k | \frac{d}{dk} | u_k \rangle$ and $|u_k\rangle$ the occupied Bloch states^{45,46}. Due to the protection of the symmetries in BDI class the Berry phase $\gamma \bmod 2\pi$ can have two values: π for a topologically nontrivial phase and 0 for a topologically trivial phase. The topological property is manifested by the boundary states of zero energy on an open chain. The spin-down subsystem, which is the time-reversal counterpart of Eq.(2), has a winding number $\nu = -1$. Then the combined system is time-reversal invariant with the time-reversal operator (the time-reversal operator \mathcal{T} is the same as the one for Eq.(1)). Then the combined system belongs to DIII class and its topological invariant is a Z_2 . The Z_2 topological invariant for s_z conserved system can be calculated using the berry phase of either spin subsystem.

III. THE OSCILLATORY CROSSOVER FROM 2D TO 1D TOPOLOGICAL PHASES

We consider the 2D TI model Eq.(1) in a narrow strip configuration. Its finite-size effect has been studied previously⁴⁷. It is found that on a narrow strip the edge states on the two sides can couple together to produce a gap in the spectrum. The finite-size gap $\Delta \propto e^{-\lambda L}$, decays in an exponential law with the width L . The decaying length scale is determined by the bulk gap of Eq.(1). As shown in Fig.2, the bulk gap vanishes at $M/B = 0, -4, -8$, near which the finite-size gap is maximum. Interestingly the narrow strip as a quasi-1D system shows 1D topological phase in an oscillatory way. It is a 1D topological phase with boundary states when the width L is odd, while trivial when the width L is even. Since spin s_z is conserved in Eq.(1), the oscillatory crossover happens also for each spin subsystem. If the spins are coupled (such as by the Rashba spin-orbit coupling described in Sec. V), the above results still persist.

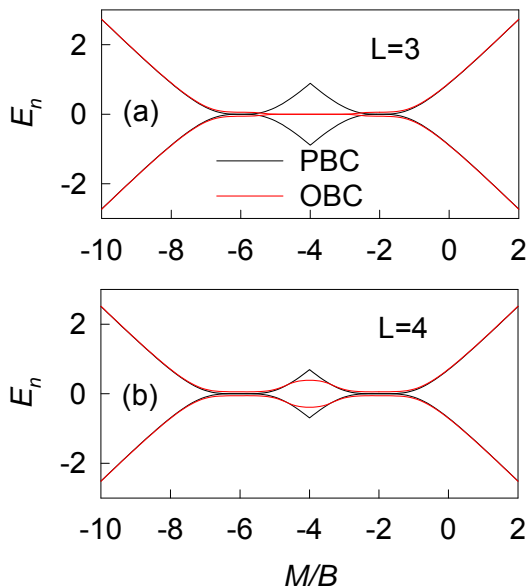


FIG. 2: (Color online) The eigenenergies at half filling and the one above of Eq.(1) vs. M on a thin strip with the width: (a) $L = 3$; (b) $L = 4$. The length of the strip is $N = 50$ with periodic boundary condition (PBC) or open boundary condition (OBC).

The oscillatory behavior happens near $M/B = -4$, where the bulk gap is zero and separates two TI phases. However it is absent near $M/B = 0, -8$, which separate a TI from a trivial insulator. It is noted in Fig.1 that $M/B = -4$ is deep in the 1D topological phase of Eq.(2), which is reduced from Eq.(1). So the oscillatory behavior is closely related to the corresponding 1D topological phase. In the following section, we construct the 2D TI model Eq.(1) from the point of view of coupled 1D models Eq.(2) to understand the oscillatory behavior.

IV. CONSTRUCTING A 2D MODEL FROM 1D TOPOLOGICAL MODEL

The 2D model in Eq.(1) can be viewed as a set of the coupled 1D models in Eq.(2). In the limit of zero coupling, the boundary states of the 1D topological model form two flat bands at the two edges of the 2D system, which are topological protected by the symmetry of the isolated 1D model. Next we study the evolution of the boundary states as the 1D chains are coupled by the hopping terms. Suppose the Hamiltonian of a 1D open chain along x - direction is $H_{1D}^{open,n}$ [the same as the one in Eq.(2)] with n denoting the n -th chain (it is identical for different n). Since the Hamiltonian $H_{1D}^{open,n}$ has the chiral symmetry, its eigenenergies are symmetric to 0 and we label them: $\{E\}_n = -E_0^{(n)}, E_0^{(n)}, -E_1^{(n)}, E_1^{(n)}, \dots (E_0^{(n)} < E_1^{(n)} \dots)$, which correspond to the eigenstates: $\{\varphi\}_n = \varphi_0^{n,-}, \varphi_0^{n,+}, \varphi_1^{n,-}, \varphi_1^{n,+}, \dots$. For the 2D system containing N_y 1D chains, we choose the basis: $\Phi = (\{\varphi\}_0, \{\varphi\}_1, \dots, \{\varphi\}_{N_y})$. Under this basis, the 2D Hamiltonian can be calculated and has the following structure,

$$H_{2D}^{(N_y)} = \begin{pmatrix} H_{diag} & H_{ndiag} & 0 & \dots \\ H_{ndiag}^\dagger & H_{diag} & H_{ndiag} & \dots \\ 0 & H_{ndiag}^\dagger & H_{diag} & \dots \\ 0 & 0 & H_{diag} & \dots \end{pmatrix},$$

where $H_{diag} = \langle \{\varphi\}_n | H_{1D}^{open,n} | \{\varphi\}_n \rangle$ is the diagonal matrix with the diagonal elements $\{E\}_n$; $H_{ndiag} = \langle \{\varphi\}_n | H_{couple} | \{\varphi\}_{n+1} \rangle$ with H_{couple} which describes the coupling between nearest-neighbor (NN) chains. H_{ndiag} contains the hopping amplitudes of the eigenstates between the NN chains, and generally one eigenstate couples with all other eigenstates of the NN chain.

We firstly consider a special case $M = -4B$, when the zero modes ($E_0^{(n)} = 0$) of the 1D open chain distribute only on the end sites. Each chain has two zero modes, one of which is on one end and the other is on the other end. When only the A -kind hoppings with the amplitude A couple the chains, the zero modes only couple the zero modes on the same end of the NN chain and the amplitude is $\pm IA$. So the low-energy physics is described by the zero modes which hop on the edge with the amplitude $\pm IA$.

For the case of two chains, we have two zero modes on each side. We can limit to a subspace composed of the zero modes, i.e., $(\varphi_0^{1,-}, \varphi_0^{2,-})$. Under this basis, the effective Hamiltonian becomes a 2×2 matrix:

$$H_{eff}^{(2)} = \begin{pmatrix} 0 & iA \\ -iA & 0 \end{pmatrix},$$

Its eigenenergy is $E_{eff}^{(2)} = \pm A$ and the system is gapped. Similarly for the case of three chains, under the basis $(\varphi_0^{1,-}, \varphi_0^{2,-}, \varphi_0^{3,-})^T$, the effective Hamiltonian becomes a

3×3 matrix:

$$H_{eff}^{(3)} = \begin{pmatrix} 0 & iA & 0 \\ -iA & 0 & iA \\ 0 & -iA & 0 \end{pmatrix}.$$

This matrix has an eigenenergy 0 with the eigenvector $\psi_0 = \frac{1}{\sqrt{2}}(\varphi_0^{1,-} + \varphi_0^{2,-})$. For the case of multi-chains, the resulting effective matrix has similar structure, i.e., a tridiagonal matrix with zero diagonal elements. The eigenenergy of such Hermitian matrix is symmetric to 0. So if the dimension of the matrix is odd, it must have the eigenvalue 0. The above result can be understood qualitatively: since two coupled boundary states tend to destroy each other, one can survive from odd number of boundary states.

The above result persists when finite B -kind hopping is included. The B -kind hopping couple the zero modes with a few other modes. For relatively small B , the coupling among the zero modes still dominates. A proper unitary transformation can move the few coupled modes to one side of the matrix, and the zero modes to the other side. If the length of the chain is long enough, i.e., the dimension of the matrix is big enough, their effect on the zero modes can be neglected, which is known as the finite-size effect. So the oscillating behavior of the topological property of quasi-1D strip created by narrowing a 2D TI can be understood in the above way.

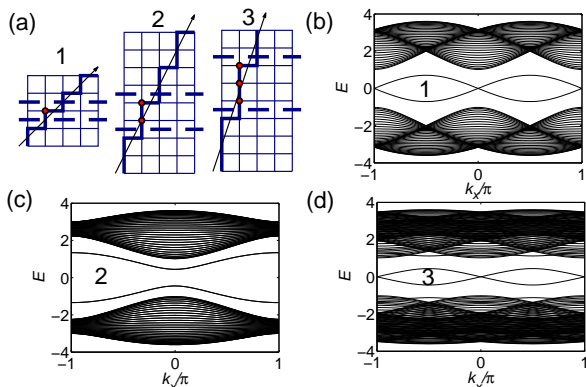


FIG. 3: (Color online) One-dimensional energy bands for a strip with different edges. The parameters are: $M = -3B$, $B' = 0$, when the system is in the WTI 1 phase.

In a general case of N_y , the zero modes form a 1D conducting chain and its energy spectrum is: $E = 2A \sin(k_y)$ with $k_y = 2\pi/N_y$ (the open boundary condition along x -direction and the periodic boundary condition along y -direction). The edge state is a mid-gap one. Specially the above edge states appear on the edge along the y -direction, but disappear on the edge along x -direction. For other kinds of edges, they can be understood from the view of coupling thin strips. As an example, we consider there different edges shown in Fig.3 (a). There are mid-gap edge states on the edges 1 and 3, but there are not on the edge 2. The thin strip in the x -direction is shown

by the dashed lines in the figure. For the system with the edge 2, the thin strip contains two chains. As discussed in the previous section, the boundary modes are gapped, thus there are no mid-gap edge states when the thin strips are coupled along the y -direction. While for the system with the edges 1 or 3, the thin strip contains odd number of chains. So the boundary modes persist and there are mid-gap edge states.

Since the bulk system is gapped, the appearance of the mid-gap edge states on specific boundaries is due to the topological property of the bulk insulator. However it is in contrast to the topological property of quantum spin Hall insulators, where there are always gapless edge states traversing the gap. The topological invariant of the above bulk system is $Z_2 = 0$, which is trivial. However the above phase is different from a trivial insulator. This implies that for 2D time-reversal invariant insulators besides the trivial insulators and the quantum spin Hall insulators, there exist another insulators, in which $Z_2 = 0$, but the mid-gap edge states appear on specific boundaries. It is somehow similar to the 3D weak TI phase, which can be understood as layered quantum spin Hall effect. So we term the above phase as '2D weak TI'.

V. THE 2D WEAK TI

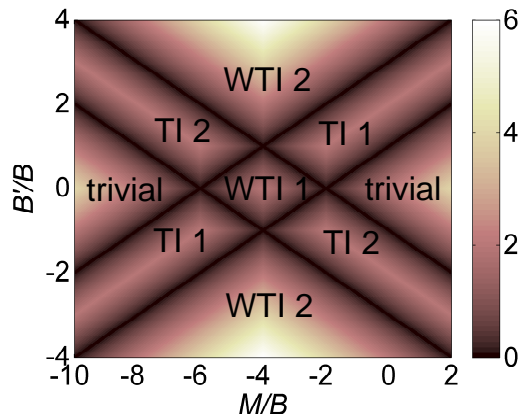


FIG. 4: The phase diagram of the modified Hamiltonian Eq.(1) with anisotropic B -kind hoppings in the (M, B') plane. In TI 1 (TI 2) the crossing of the edge states is at $k_y = 0(\pi)$ with y -directed boundary. The color represents the gap of the bulk system.

In the previous section a weak 2D TI is identified with the mid-gap edge states along specific edges and the topological invariant $Z_2 = 0$. More generally the Hamiltonian in Eq.(1) can be modified by changing the amplitude of the B -kind hopping along y -direction to B' which can be tuned. With the points on which the gap closes, the phase diagram of the modified Hamiltonian in the (M, B') plane can be obtained. As shown in Fig.4, besides the quantum spin Hall insulators and trivial insulators, the 2D weak TI exists in three regions of the phase

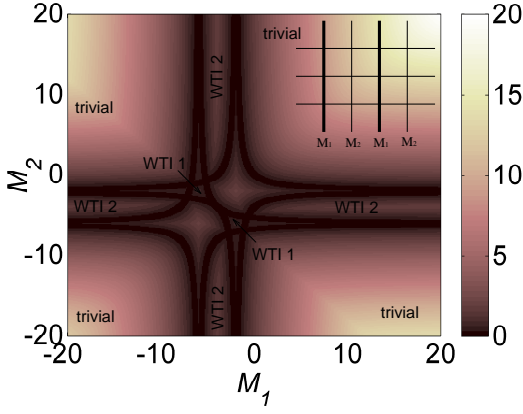


FIG. 5: The phase diagram of the modified Hamiltonian Eq.(1) with anisotropic mass in the (M_1, M_2) plane. The inset schematically shows the pattern of the mass on the lattice. The regions without notation represent the quantum spin Hall insulator. The color represents the gap of the bulk system.

diagram. We distinguish the 2D weak TIs with the mid-gap edge states appearing on x - edge (WTI 2) or y - edge (WTI 1), and the quantum spin Hall insulators with the gapless crossing appearing at $k_y = 0$ (TI 1) or $k_y = \pi$ (TI 2).

It is noticed that the 2D weak TI exists in the regions with anisotropic B -kind hoppings ($B' \neq B$). Indeed the anisotropy is key to realize the phase⁴⁸. The anisotropy can also be induced in the parameter M of Eq.(1). Consider the case shown in Fig.5: the mass M is uniform along y - direction, but has alternating values M_1, M_2 along x - direction. The phase diagram in the (M_1, M_2) plane is shown in Fig.5, in which the 2D weak TI is identified in six regions.

Till now the 2D weak TI is identified in the anisotropic systems. Its topological invariant Z_2 is zero, but the phase is different from the $Z_2 = 0$ trivial insulators. It is desirable to characterize its topological property. It has been known that the Z_2 topological invariant of a 2D time-reversal invariant insulator is defined as: $(-1)^{\nu_0} = \prod_{n_j=0,1} \delta_{n_1 n_2}$, with $\delta_{n_1 n_2}$ the time-reversal polarization at the four time-reversal invariant momenta $\Gamma_{i=(n_1 n_2)} = (n_1 \pi \hat{x} + n_2 \pi \hat{y})$, with $n_j = 0, 1$. The above constructed 2D Hamiltonian has the inversion symmetry $H(-\mathbf{k}) = \hat{P}H(\mathbf{k})\hat{P}$ with \hat{P} the inversion operator. In the presence of the inversion symmetry, δ_i can be determined by the parity of the occupied band eigenstates: $\delta_i = \prod_{m=1}^N \xi_{2m}(\Gamma_i)$, where ξ_{2m} is the parity eigenvalues of the $2m$ -th occupied states. The topological property of 2D time-reversal invariant insulators is determined by four time-reversal polarizations δ_i . In general δ_i is not gauge invariant, while in the presence of inversion symmetry δ_i is gauge invariant. So for the $Z_2 = 0$ time-reversal invariant insulators with inversion symmetry, the details of the four δ_i should distinguish the 2D weak TIs and the trivial insulators.

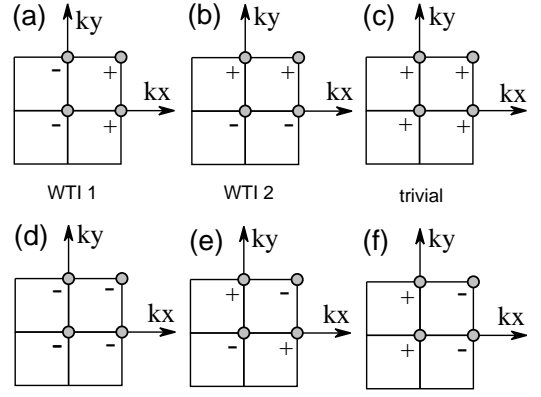


FIG. 6: Depicts δ_i at the time-reversal invariant momenta of 2D weak TIs and trivial insulators. The upper ones are for the case of anisotropic B -kind hoppings: (a) WTI 1;(b) WTI 2;(c) trivial insulator. The lower ones are for the case of anisotropic mass: (d) WTI 1;(e) WTI 2;(f) trivial insulator.

For the case of anisotropic B -kind hoppings, the inversion operator is $\hat{P} = I \otimes \sigma_Z$ and $\delta_i = -\text{sgn}(M(\Gamma_i))$ with $\tilde{M}(\mathbf{k}) = M + 4B - 2B \cos(k_x) - 2B' \cos(k_y)$. In WTI 1, if the boundary is along y - direction, the two δ_i projected on $k_y = 0(\pi)$ have different signs, which is in contrast to the trivial insulator. Define the Z_2 invariant π_{k_μ} the product of two δ_i on the line k_μ ($k_\mu = n_i \pi, \mu = x, y$), then the additional Z_2 indices π_{k_μ} distinguish the 2D weak TI and trivial insulators. π_{k_μ} is directly related to the existence of the edge states on μ -directed boundary and $\pi_{k_\mu} = -1$ means a crossing of the edge states at k_μ . For example in the WTI 1 phase shown in Fig.6(a), if the boundary is along y - direction, k_y remains good quantum number and $\pi_{k_y=0} = \pi_{k_y=\pi} = -1$. So there appear mid-gap edge states with two crossings at $k_y = 0, \pi$ on the boundaries. Also in quantum spin Hall insulators, π_{k_μ} determines the position of the crossing of the edge states, which happens at k_μ with $\pi_{k_\mu} = -1$.

For the case of anisotropic mass, the inversion operator is $\hat{P} = I \otimes \text{diag}(\sigma_z, e^{-ik_y/2} \sigma_z)$ (the inversion center is chosen on a site with the mass M_1). The δ_i of the 2D weak TI phases are calculated, which is shown in Fig.6. It seems that the above discussion is inapplicable. Actually to characterize the topological property properly, the δ_i should be defined compared to the corresponding $\delta_i^{\text{trivial}}$ of the trivial insulator in the same model, i.e., $\tilde{\delta}_i = \delta_i \delta_i^{\text{trivial}}$. With $\tilde{\delta}_i$, Fig.6(d) [(e)] is the same as Fig.6(a) [(b)], and the 2D weak TI is characterized correctly.

So to correctly characterize the 2D weak TI with inversion symmetry, the δ_i should be defined compared to that of the trivial insulator in the same model. It can be understood from the view of band inverting. We take the case of anisotropic mass as an example. Its Hamiltonian in the momentum space writes as,

$$H_M(\mathbf{k}) = \begin{pmatrix} h_1(k_y) & h_{12}(k_x) \\ h_{12}^\dagger(k_x) & h_2(k_y) \end{pmatrix}, \quad (3)$$

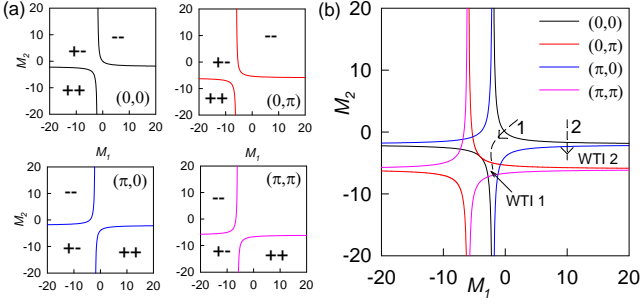


FIG. 7: (Color online) (a) The zero-gap line in (M_1, M_2) plane for the case of anisotropic mass at the four time-reversal invariant momenta. $+/-$ is the parity of the occupied band. (b) The phase diagram obtained by combining the zero-gap lines in (a). The arrow dashed line 1(2) is the path to WTI 1(2) (the ones corresponding to (d) and (e) in Fig.6) from a trivial insulator.

where $h_{1,2}(k_y) = [M_{1,2} + 4B - 2B \cos(k_y)]\sigma_z + 2A \sin(k_y)\sigma_x$ and $h_{12}(k_x) = -B(1 + e^{-ik_x})\sigma_z - iA(1 - e^{-ik_x})\sigma_y$. The eigenenergies and eigenvectors at the time-reversal invariant momenta can be obtained analytically. In Fig.7 (a) the zero-gap line in the (M_1, M_2) plane at each time-reversal invariant momentum and the parities of the occupied bands are shown. When the zero-gap line is crossed, there occurs a band inverting. By combining all the zero-gap lines, the phase diagram in Fig.5 is recovered. Any phase in the phase diagram can be reached by band inverting starting from a trivial insulator. Thus $\tilde{\delta}_i = \delta_i \delta_i^{trivial}$ records the number of band inverting from a trivial insulator. $\tilde{\delta}_i = -1$ means an odd number of band inverting and there appears a crossing of the edge state at i -th time-reversal invariant momentum. Then the topological property can be analyzed correctly with $\tilde{\delta}_i$.

For the general case without inversion symmetry, the topological property of the 2D weak TI can be understood from the Berry phase of one spin subsystem, since the 2D weak TI is closely related to 1D topological phase. The Berry phase defined with $k_y(k_x)$ at fixed $k_x(k_y)$ can be calculated. The symmetries which protects the 1D topological phase is broken except at specific $k_x(k_y)$. If there are two $k_x(k_y)$ at which the Berry phase is π , which means the edge states exist and have two crossings in the presence of $x(y)$ -directed boundary, the system is a 2D weak TI.

The above analysis is based on the system with spin s_z conservation. However the result is applicable to any time-reversal invariant insulators. Next we study the case of the spin-up and -down subsystem coupled by Rashba spin-orbit coupling, which preserve the time-reversal invariant symmetry,

$$H_R = - \sum_{i, \hat{x}} sgn(\hat{x}) i \lambda_R \Psi_i^\dagger s_y \otimes I \Psi_{i+\hat{x}} \quad (4)$$

$$+ \sum_{i, \hat{y}} sgn(\hat{y}) i \lambda_R \Psi_i^\dagger s_x \otimes I \Psi_{i+\hat{y}}.$$

Adding the above term to the modified version of the Hamiltonian Eq.(1). For the case of anisotropic B -kind hoppings, the total Hamiltonian in the momentum space is,

$$H_T(\mathbf{k}) = \tilde{M}(\mathbf{k})I \otimes \sigma_z + \tilde{A}(k_x)s_z \otimes \sigma_x + \tilde{A}(k_y)I \otimes \sigma_y + \tilde{\lambda}_R(k_x)s_y \otimes I - \tilde{\lambda}_R(k_y)s_x \otimes I. \quad (5)$$

Its energy spectrum is:

$$(E_T(\mathbf{k}))^2 = [\tilde{A}(k_x)]^2 + \{\pm \sqrt{[\tilde{\lambda}_R(k_x)]^2 + [\tilde{\lambda}_R(k_y)]^2} + \sqrt{[\tilde{M}(\mathbf{k})]^2 + [\tilde{A}(k_y)]^2}\}^2. \quad (6)$$

with $\tilde{A}(k_x) = 2A \sin(k_x)$, $\tilde{A}(k_y) = 2A \sin(k_y)$, $\tilde{\lambda}_R(k_x) = 2\lambda_R \sin(k_x)$, $\tilde{\lambda}_R(k_y) = 2\lambda_R \sin(k_y)$. As has been known, the Rashba spin-orbit coupling does not break the quantum spin Hall effect when it is small. In the following we show that the weak TI is also robust to it. From Eq.(6), it is noticed that the gap closing is independent of λ_R for $\lambda_R < A$. Since the topological quantum phase transition occurs when the gap closes, the weak TI is not affected by the Rashba spin-orbit coupling in this case. For $\lambda_R > A$, the gap of the bulk system vanishes at a critical λ_R^c , when the weak TI is broken. The calculated energy spectrum and time-reversal polarization δ_i are consistent with the above analysis. For the case of anisotropic mass, the result is similar.

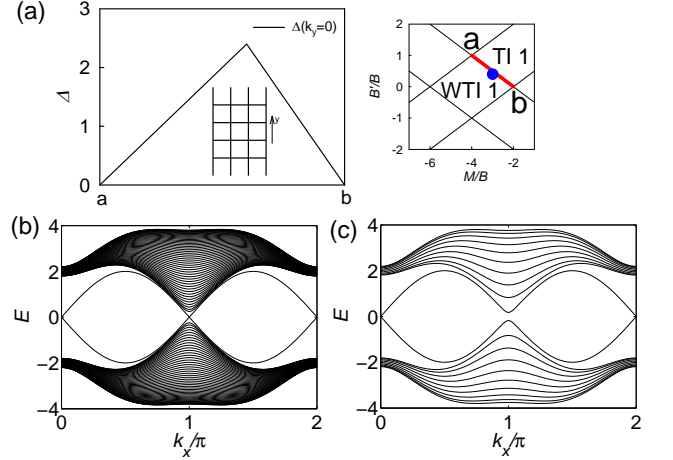


FIG. 8: (Color online) (a) The bulk gap at $k_y = 0$ with the parameters along the boundary of WTI 1 and TI 1 in the phase diagram (the bulk gap at $k_y = \pi$ is all zero). The energy spectrum on a y -directed strip with the width: (b) $L = 50$ and (c) $L = 10$. The parameters are: $M/B = -3, B'/B = 0.4$, which is denoted by a blue dot in the right figure of (a) and it is in the WTI 1 phase near the boundary.

As has been stated, since the mid-gap edge states in the 2D weak TI are related to the corresponding 1D boundary modes, it can be destroyed by the disorder. However under specific conditions, they can be robust as those in the $Z_2 = 1$ quantum spin Hall insulators. It can happen

in the region near the boundary between WTI and TI phases. For example, for the case with anisotropic B -kind hoppings, in the middle of the boundary between WTI and TI phases, the gaps at the two valleys $k_{x(y)} = 0, \pi$ is different. For the case shown in Fig.8, the gap at $k_y = \pi$ is nearly zero while is still large at $k_y = 0$. Considering a narrow strip with its edges along y - direction, due to the finite-size effect, the edge states at $k_y = \pi$ is gapped, while the ones at $k_y = 0$ persist. Thus a single robust gapless crossing at $k_y = 0$ is realized in the finite-size gap.

VI. CONCLUSIONS AND DISCUSSIONS

Dimensional evolution between $1D$ and $2D$ topological phases is investigated systematically. The crossover from a $2D$ TI to its $1D$ limit shows oscillatory behavior between a $1D$ ordinary insulator and $1D$ TI. By constructing a $2D$ topological system from $1D$ TI, it is shown that there exist the weak topological phase in $2D$ time-reversal invariant band insulators. The phase can be realized in anisotropic systems. In the weak phase, the topological invariant $Z_2 = 0$ and the edge states only appear along specific boundaries. Since the edge states are closely related to the boundary states of the corresponding $1D$ topological phase, they may be destroyed by disorder and have symmetry-protecting nature as the corresponding $1D$ topological phase. The effect of the Rashba spin-orbit coupling, which preserves time-reversal invari-

ant symmetry, but couples the spins, is also studied. These results provide further understanding on $2D$ time-reversal invariant insulators.

Finally we discuss the relevance of the results to experimental measurements. It is unclear whether the $2D$ weak TI materials exist in nature. However since the anisotropy is important, it should be searched in anisotropic materials. Besides real materials, recently the double-well potential formed by laser light has been developed⁴⁹, in which s and p orbital cold-atoms can be loaded. It has been shown that a $1D$ topological model similar to Eq.(2) can be derived from the experimentally realized double-well lattices by dimension reduction³⁹. Another experimental platform is the photonic quasicrystals, on which the topological properties have been studied in an engineered way³⁶. With the fine tuning of the parameters and the geometries in these experiments, the present results are very possibly realized experimentally.

Acknowledgments

The authors thank Hua Jiang and Juntao Song for helpful discussions. This work was supported by NSFC under Grants No.11274032 and No. 11104189, FOK YING TUNG EDUCATION FOUNDATION, Program for NCTE (H.M.G), and the Research Grant Council of Hong Kong under Grant No. HKU 703713P (S.Q.S).

Note added.- Upon finalizing the manuscript we noticed a recent preprint⁵⁰ on closely related topics.

-
- ¹ hmguo@buaa.edu.cn.
² J. E. Moore, Nature **464**, 194 (2010).
³ M. Z. Hasan and C. L. Kane, Rev. Mod. Phys. **82**, 3045 (2010).
⁴ X. L. Qi and S. C. Zhang, Rev. Mod. Phys. **83**, 1057 (2011).
⁵ S. Q. Shen, Topological Insulators (Springer, Berlin, 2012).
⁶ C. L. Kane and E. J. Mele, Phys. Rev. Lett. **95**, 146802 (2005).
⁷ C. L. Kane and E. J. Mele, Phys. Rev. Lett. **95**, 226801 (2005).
⁸ L. Fu and C. L. Kane, Phys. Rev. Lett. **98**, 106803 (2007).
⁹ L. Fu and C. L. Kane, Phys. Rev. B **76**, 045302 (2007).
¹⁰ H. Zhang, C.-X. Liu, X.-L. Qi, X. Dai, Z. Fang, and S. C. Zhang, Nat. Phys. **5**, 438 (2009).
¹¹ D. Hsieh, D. Qian, L. Wray, Y. Xia, Y. S. Hor, R. J. Cava, and M. Z. Hasan, Nature (London) **452**, 970 (2008).
¹² Y. Xia, D. Qian, D. Hsieh, L. Wray, A. Pal, H. Lin, A. Bansil, D. Grauer, Y. S. Hor, R. J. Cava, and M. Z. Hasan, Nat. Phys. **5**, 398 (2009).
¹³ H. Lin, L. A. Wray, Y. Xia, S. Xu, S. Jia, R. J. Cava, A. Bansil, and M. Z. Hasan, Nat. Mater. **9**, 546 (2010).
¹⁴ Y. L. Chen, J. G. Analytis, J. H. Chu, Z. K. Liu, S. K. Mo, X. L. Qi, H. J. Zhang, D. H. Lu, X. Dai, Z. Fang, S. C. Zhang, I. R. Fisher, Z. Hussain, Z. X. Shen, Science **325**, 178 (2009).
¹⁵ B. A. Bernevig, T. L. Hughes, and S.-C. Zhang, Science **314**, 1757 (2006).
¹⁶ M. König, S. Wiedmann, C. Brune, A. Roth, H. Buhmann, L. W. Molenkamp, X. L. Qi, and S. C. Zhang, Science **318**, 766 (2007).
¹⁷ I. Knez, R.-R. Du, and G. Sullivan, Phys. Rev. Lett. **107**, 136603 (2011).
¹⁸ C. X. Liu, H. J. Zhang, B. H. Yan, X. L. Qi, T. Frauenheim, X. Dai, Z. Fang, and S. C. Zhang, Phys. Rev. B **81**, 041307 (2010).
¹⁹ H. Z. Lu, W. Y. Shan, W. Yao, Q. Niu, and S. Q. Shen, Phys. Rev. B **81**, 115407 (2010).
²⁰ Y. Zhang, K. He, C. Z. Chang, C. L. Song, L. L. Wang, X. Chen, J. F. Jia, Z. Fang, X. Dai, W. Y. Shan, S. Q. Shen, Q. Niu, X. L. Qi, S. C. Zhang, X. C. Ma, and Q. K. Xue, Nat. Phys. **6**, 584 (2010).
²¹ P. Cheng, C. L. Song, T. Zhang, Y. Y. Zhang, Y. L. Wang, J. F. Jia, J. Wang, Y. Y. Wang, B. F. Zhu, X. Chen, X. C. Ma, K. He, L. L. Wang, X. Dai, Z. Fang, X. C. Xie, X. L. Qi, C. X. Liu, S. C. Zhang, and Q. K. Xue, Phys. Rev. Lett. **105**, 076801 (2010).
²² R. Yu et al., Science **329**, 61 (2010).
²³ C. Z. Chang et al., Science **340**, 167 (2013).
²⁴ J. Wang, B. Lian, H. J. Zhang, Y. Xu, and S. C. Zhang, Phys. Rev. Lett. **111**, 136801 (2013).
²⁵ H. Jiang, Z. H. Qiao, H. W. Liu, and Q. Niu, Phys. Rev. B **85**, 045445 (2012).
²⁶ G. Yang, J. W. Liu, L. Fu, W. H. Duan, and C. X. Liu, arXiv: 1309.7932 (2013).

- ²⁷ B. H. Yan, L. Mchler, and C. Felser, *Phys. Rev. Lett.* **109**, 116406 (2012).
- ²⁸ P. Z. Tang, B. H. Yan, W. D. Cao, S. C. Wu, C. Felser, and W. H. Duan, arXiv: 1307.8054 (2013).
- ²⁹ R. S. K. Mong, J. H. Bardarson, and J. E. Moore, *Phys. Rev. Lett.* **108**, 076804 (2012).
- ³⁰ H. Jiang, H. W. Liu, J. Feng, Q.F. Sun, and X. C. Xie, *Phys. Rev. Lett.* **112**, 176601 (2014).
- ³¹ T. Das and A. V. Balatsky, *Nat. Commun.* **4**, 1972 (2013).
- ³² L. J. Lang, X. M. Cai, and S. Chen, *Phys. Rev. Lett.* **108**, 220401 (2012).
- ³³ H. M. Guo and S. Q. Shen, *Phys. Rev. B* **84**, 195107 (2011).
- ³⁴ H. M. Guo, S. Q. Shen, and S. P. Feng, *Phys. Rev. B* **86**, 085124 (2012).
- ³⁵ H. M. Guo, *Phys. Rev. A* **86**, 055604 (2012).
- ³⁶ Y. E. Kraus, Y. Lahini, Z. Ringel, M. Verbin, and O. Zeitlinger, *Phys. Rev. Lett.* **109**, 106402 (2012).
- ³⁷ M. Atala, M. Aidelsburger, J. T. Barreiro, D. Abanin, T. Kitagawa, E. Demler, and I. Bloch, *Nat Phys* **9**, 795 (2013).
- ³⁸ W. Tan, Y. Sun, H. Chen and S. Q. Shen, *Scientific Reports* **4**, 3842 (2014).
- ³⁹ X. P. Li, E. H. Zhao and W. V. Liu, *Nat. Commun.* **4**, 1523 (2013).
- ⁴⁰ S. Q. Shen, W. Y. Shan and H. Z. Lu, *SPIN* **01**, 33 (2011).
- ⁴¹ A. P. Schnyder, S. Ryu, A. Furusaki, and A. W. W. Ludwig, *Phys. Rev. B* **78**, 195125 (2008).
- ⁴² D. Sticlet, L. Seabra, F. Pollmann and J. Cayssol, *Phys. Rev. B* **89**, 115430 (2014).
- ⁴³ I. M. Shem, T.L. Hughes, J.T. Song and E. Prodan, arXiv: 1311.5233 (2013).
- ⁴⁴ J.T. Song, E. Prodan, arXiv: 1402.7116 (2014).
- ⁴⁵ R. Resta, *Rev. Mod. Phys.* **66**, 899 (1994).
- ⁴⁶ D. Xiao, M.C. Chang, and Q. Niu, *Rev. Mod. Phys.* **82**, 1959 (2010).
- ⁴⁷ B. Zhou, H. Z. Lu, R. L. Chu, S. Q. Shen, Q. Niu, *Phys. Rev. Lett.* **101**, 246807 (2008).
- ⁴⁸ T. Fukui, K. I. Imura, and Y. Hatsugai, *J. Phys. Soc. Jpn.*, **82**, 073708 (2013).
- ⁴⁹ J. Sebby-Strabley, M. Anderlini, P. S. Jessen, and J. V. Porto, *Phys. Rev. A* **73**, 033605 (2006).
- ⁵⁰ Y. Yoshimura, K.-I. Imura, T. Fukui, Y. Hatsugai, arXiv: 1405.4842 (2014).